Yang, L., Zhao, M., Gardner, L., Ning, K. and Wang, J. (2019). Member stability of stainless steel welded I-section beam-columns. Journal of Constructional Steel Research, 155: 33-45.

Member stability of stainless steel welded I-section beam-columns

Lu Yang[a,*], Menghan Zhao[a], Leroy Gardner[b], Keyang Ning[a], Jie Wang[c]

[a]*The Key Laboratory of Urban Security and Disaster Engineering of Ministry of Education, Beijing University of Technology, Beijing 100124, China*
[b]*Dept. of Civil and Environmental Engineering, Imperial College London, London, UK*
[c]*Dept. of Architecture & Civil Engineering, University of Bath, Bath, UK*

Abstract: A comprehensive experimental and numerical study is presented into the behaviour of stainless steel welded I-section beams-columns. Twenty test specimens were fabricated from grade 304 (EN 1.4301) austenitic and grade 2205 (EN 1.4406) duplex stainless steel plates – ten were tested under major axis bending plus compression and ten under minor axis bending plus compression. Material tensile coupon tests and geometric imperfection measurements were also conducted. Numerical models were developed, calibrated against the test results and subsequently employed in parametric studies considering a wider range of specimen geometries. Based on the obtained test and numerical results, the accuracy and reliability of existing design rules given in EN 1993-1-4 and AISC DG 27, as well as recent proposals, were assessed.

Keywords: stainless steel; beam-columns; flexural buckling; welded I-section; numerical study

* Corresponding author.
E-mail: lyang@bjut.edu.cn (L Yang)

1. Introduction

Recent research into the structural performance of stainless steel has led to a greatly improved understanding of the material properties [1-4], cross-sectional behaviour [4-10] and column buckling response [11-15], providing valuable knowledge for the development of accurate structural design rules. For stainless steel beam-columns, research has been performed on a range of grades (austenitic [16-18], ferritic [19] and duplex [20-23]), fabrication processes (cold-formed [16,19-23], conventionally welded [16] and laser-welded [17]) and cross-section shapes (built-up I-sections [16-18], circular hollow sections [18] and square and rectangular hollow sections [16, 19-23]). Design rules for stainless steel beam-columns are included in the European design code EN 1993-1-4 [24] and the American design standards SEI/ASCE 8-02 [25] and AISC DG 27 [26]. The accuracy of these design provisions has been assessed in a number of recent studies [17, 19-21, 27], where scope for improvement was revealed and new design proposals were made.

Among previous research studies into the structural performance of stainless steel elements, welded I-section beam-columns remain relatively unexplored. To address this, a comprehensive experimental and numerical study into the behaviour of austenitic and duplex stainless steel welded I-section members subjected to compression and uniaxial bending is presented herein.

A total of 20 beam-column tests, with a number of combinations of compression plus bending about the major and minor axes, was carried out. Numerical models were also developed and validated against the test results, and subsequently used in parametric studies to generate results over a wider range of cross-section and member slendernesses. The obtained test and FE results were used in the evaluation of existing design rules for stainless steel beam-columns with welded sections given in the European standard EN 1993-1-4 [24], the American Design Guide AISC DG 27 [26] and proposed in a recent study [17].

2. Experimental program

The experimental program performed in the current study comprised material coupon tests, measurements of geometric imperfections and beam-column tests. The beam-column specimens were built up from stainless steel plates of two grades – austenitic stainless steel grade 304 (EN 1.4301) and duplex stainless steel grade 2205 (EN 1.4462), and two nominal thicknesses – 6 mm and 10 mm for each grade. The chemical compositions of each grade and thickness, as obtained from the mill certificates, are given in Table 1. The reported chemical compositions meet the requirements of GB/T 222-2006 [28] for grade 304 stainless steel and GB/T 20878-2007 [29] for grade 2205 stainless steel.

2.1 Material coupon tests

To obtain the basic material constitutive relationship of the studied specimens, tensile coupon tests were carried out. The coupons were cut directly from the raw stainless steel hot-rolled plates, which were from the same batch as those used to form the specimens. For each grade and each thickness, three coupons were cut along the rolling direction of the plate, resulting in a total of 12 tensile coupons. The dimensions of the coupons are shown in Fig. 1.

The tensile coupon tests were conducted in a 300 kN electro-hydraulic testing machine (Fig. 2) following the procedure set out in EN ISO 6892-1-2009 [30]. The material stress was obtained from the machine load (with an accuracy of ±0.25%) divided by the cross-sectional area of the coupon, A_c, and the strain was recorded using an extensometer with a gauge length of 50 mm, until the measurement range was exceeded. The measured stress-strain curves of all the coupons are reported in Fig. 3, where it shows that no sharply defined yield point can be identified for all the materials, evidencing the nonlinear characteristics of stainless steel. Table 2 summarises the average values of the key measured material parameters, including the Young's modulus, E, the 0.2% proof stress, $f_{0.2}$, the ultimate tensile stress, f_u, the strain-hardening exponent, n, the strain at the ultimate tensile stress, ε_u, and the plastic strain at fracture, ε_f, which was measured as the elongation over the standard gauge length of $5.65\sqrt{A_c}$ using the fractured tensile coupons [30].

2.2 Specimen fabrication

The I-section beam-column specimens were built-up (i.e. welded) from hot-rolled plates of two

stainless steel grades (304 and 2205). Two cross-section sizes were fabricated – I-120×150×10×6 (tested under compression plus major axis bending) and I-140×150×10×6 (tested under compression plus minor axis bending), with the four numbers in the section designation corresponding to section height H, section width B, flange thickness t_f and web thickness t_w, respectively – see Fig. 4. The constitutive plates of each specimen were first laser-cut and then welded together using shielded metal arc welding, with fillet welds of 6 mm throat thickness. To match the parent materials, welding rods of grades E308 and E2209 were applied to the 304 and 2205 materials, respectively. All the specimens were straightened after welding. To facilitate the adopted beam-column loading condition of eccentric compression, Q345 steel plates were welded to both ends of each specimen, offset from the centreline of the specimen by the loading eccentricity required in each test, as illustrated in Fig. 5.

A total of 20 beam-column specimens was fabricated. The measured dimensions and loading eccentricity of each specimen, along with the axis of bending, are given in Table 3, where L is the length of the specimen measured between the end-plates and e_m is the applied load eccentricity, measured as the average distance between the centreline of the specimen and that of the end-plates at each end (Fig. 5). The effective lengths L_e of the test specimens, measured between the knife edges are also reported in Table 3; these were calculated as $L_e = L + (170\text{ mm} \times 2)$, with 170 mm being the distance between the specimen ends and knife edges at each end. The tested cross-sections were either Class 1 or 3 according to the classification limits of EN 1993-1-4 [24]. The non-dimensional lateral-torsional buckling slenderness [24] of the members bent about the major axis was less than 0.4, meaning that lateral-torsional buckling was not expected. In the adopted specimen labelling system, as used in Table 3, I and H indicate major and minor axis bending, respectively, 304 and 2205 denote the stainless steel grade, the following four-digit number represents the nominal length of the specimen, and the number 1 or 2 at the end of the label distinguishes between specimens with same dimension but different loading eccentricities (with 2 indicating higher eccentricities).

2.3 Geometric imperfection measurements

Prior to testing, measurements of initial geometric imperfections were performed on the fabricated beam-column specimens. Since local buckling was essentially precluded by the selection of the specimen geometry, only global out-of-straightness was measured in the current study. The initial global geometric imperfections were measured by means of an optical theodolite and a calibrated vernier; this method has been employed in previous similar studies (e.g. [15]). The theodolite was used to generate a virtual straight line, connecting the centrelines of the two end cross-sections, located 50 mm away from the end-plates longitudinally. The deviation of the centrelines of the mid-height cross-section and two quarter-point cross-sections, as measured by the vernier from the virtual straight line, was taken as the initial global imperfections, and denoted δ_2, δ_1 and δ_3, respectively, as schematically illustrated in Fig. 6. The maximum value δ_0 among the three measurements ($\delta_0 = \max(\delta_1, \delta_2, \delta_3)$) was adopted as the global imperfection of the specimen. A summary of the measured global geometric imperfections is provided in Table 4. It can be seen that the overall geometric imperfections of the test specimens were generally small, with the majority of the maximum amplitudes being

below L_e/1000. Specimen H 304-4000-1 had a higher imperfection, associated with excessive thermal bowing during fabrication.

2.4 Beam-column tests

2.4.1 Test set-up

The beam-column tests were performed using a 5000 kN hydraulic loading machine, as illustrated in Fig. 7. The specimens were simply-supported on knife-edges at both ends, allowing free rotation about the axis of bending. The monitored variables during the tests were the applied load, end-rotation and axial displacement at the bottom end of the speicmens, the in-plane and out-of-plane lateral displacements at mid-height, and the strains at the mid-height and end cross-sections. The load was read directly from the load cell installed within the testing machine. The end-rotation was measured through the use of two linear variable displacement transducers (LVDTs), namely LVDT-1 and LVDT-2, positioned on the bottom end-plate. The rotation was derived using the difference between the two LVDT readings and their distance apart. Since the moving head of the testing machine was located at the bottom end of the specimens, the axial displacement of the specimens was recorded by LVDT-3 and LVDT-4 attached to the bottom end-plate and positioned along the axis parallel to the knife edge to avoid the influence of the end-plate rotation on the measured axial deformation. At the mid-height of the specimen, LVDT-5 measured the out-of-plane deflection while LVDT-6 and LVDT-7 monitored the in-plane deflections. It should be noted that all the LVDTs were positioned with reference to the axis of bending, which means that the LVDT arrangement for testing about the major axis was perpendicular to that about the minor axis. The strain distribution at the mid-height cross-section and two end cross-sections (20 mm away from the end-plates) was measured using strain gauges arranged according to Fig. 8.

All the tests were initially load controlled, at a rate of 80 kN/min. After reaching the ultimate load, the test was switched to displacement control, at a rate of 20 mm/min, enabling the post-ultimate response of the test specimens to be recorded. The unloading path was followed until the load had fallen to around 60% of the ultimate load. All the readings were recorded at 1 sec intervals using a data acquisition system developed at Tsinghua University.

2.4.2 Loading eccentricity

The actual loading eccentricity e_0 applied to the test specimens can be derived using the strain gauge readings at the end cross-sections of the members through the relationship given in Eq. (1).

$$e_0 = \frac{\left(\varepsilon_1 + \varepsilon_2 - \varepsilon_3 - \varepsilon_4\right)}{4} \frac{EW_{el}}{N} \tag{1}$$

where ε_1, ε_2, ε_3, ε_4 correspond to the absolute strain readings from strain gauges SG 2-2/3-2, SG 2-4/3-4, SG 2-1/3-1 and SG 2-3/3-3 in the major axis tests and strain gauges SG 2-1/3-1, SG 2-2/3-2, SG 2-3/3-3 and SG 2-4/3-4 readings in the minor axis tests, W_{el} is the elastic modulus of

the cross-section about the relevant axis and N is the applied load. Note that e_0 should be determined during the elastic range of the tests. This procedure has been adopted in previous studies [6, 31]. The actual loading eccentricities e_0 derived from the test results in this manner are reported in Table 5 and are considered to be a more accurate reflection of the actual loading eccentricities experienced by the test specimens than the e_m values reported in Table 3, and are therefore employed in the subsequent analyses reported in this paper.

2.4.3 Test results

All the beam-column specimens failed in-plane by bending and global flexural buckling, as depicted in Figs 9(a) and 9(b) for major and minor axis bending, respectively. It should be noted that for major axis bending tests, some lateral-torsional deformations were observed, but only after the peak load was achieved. This was verified by comparing the LVDT-6 and LVDT-7 readings during the tests, which deviated from one another only after the peak load, as shown in Figs 10(a) and 10(b) for the I 304-3000-1 and I 2205-3000-1 specimens, respectively. The measured curves of load versus lateral displacement at mid-height (using the average readings from LVDT-6 and LVDT-7) for all the specimens are shown in Figs 11(a)-11(d), where Figs 11(a) and 11(b) show the curves for the 304 specimens in major and minor axis bending, respectively, while Figs 11(c) and 11(d) show the curves for the 2205 specimens in major and minor axis bending, respectively. As expected, it can be observed that the load bearing capacity decreases as the specimen length increases, while increasing the loading eccentricity is also shown to lead to a reduction in the load carrying capacity of the beam-columns. The ultimate loads achieved in the tests are summarised in Table 5.

The strain development at the critical cross-section (at mid-height) can be assessed by examining the strain gauge readings plotted against the applied load, as shown in Fig. 12, where the examples of the I 304-3000-1, H 304-3000-1, I 2205-3000-1 and H 2205-3000-2 specimens are given. As expected for beam-column members, the absolute values of the strain gauge readings on the concave (compression) side are larger than those on the convex (tensile) side. Furthermore, the strain gauge readings on the concave side of all the specimens exceeded the yield strain $\varepsilon_{0.2} = (f_{0.2}/E + 0.002)$ at failure.

3. Numerical study

Following the experimental study, finite element (FE) models were developed and validated against the test results. The validated models were then used in a subsequent parametric study to generate data over a wider range of geometric dimensions. The general-purpose FE analysis package ABAQUS [32] was employed throughout the numerical study.

3.1 Modelling assumptions

The geometries of the FE model for each specimen were established based on the measured dimensions reported in Table 3. The four-noded, reduced integration shell element S4R [32], was employed to discretise the models with a mesh size of t (where t is the material thickness)

around the cross-section and 3t in the longitudinal direction. The material stress-strain relationship was represented through a piecewise linear, isotropic hardening, constitutive model established based on the tensile coupon test results (see Fig. 3 and Table 2) with a Poisson's ratio of 0.3.

The simply-supported end conditions and the application of the eccentric load were achieved by rigidly coupling the two end cross-sections of the members to a reference point, which was offset both longitudinally and transversely according to the knife edge location in the experiments; selected degrees of freedom were released at the reference points to allow rotation about the required axis of bending and longitudinal displacement at the loaded end.

Initial geometric imperfections and residual stresses were also incorporated into the FE models. The geometric imperfection was applied in the form of the first global eigenmode with an amplitude equal to the measured imperfection δ_0 (given in Table 4) for the validation study. Residual stresses were introduced into the FE simulations through the use of the 'INITIAL CONDITIONS' command, based on a simplified representation of the models proposed in [33]. The original (shown by solid lines) [33] and simplified (shown by dashed lines) residual stress distributions are shown in Figs 13(a) and (b) for the grade 304 and 2205 materials respectively.

3.2 Validation of FE models

Typical observed failure modes from the FE models and the corresponding experiments are depicted in Figs 14(a) and 14(b) for the cases of compression plus major and minor axis bending, respectively, where good agreement may be seen. Figs 15 and 16 compare the load versus the lateral displacement at mid-height and load versus axial displacement responses, respectively, of typical test specimens and FE models. In general, the experimental load-displacement relationships were accurately captured by the FE models. Numerical comparisons of the ultimate loads achieved in the tests and FE models are also given in Table 5. The mean FE-to-test ultimate load ratios $N_{u,\mathrm{FE}}/N_{u,\mathrm{exp}}$ are 0.998 and 0.970 with coefficient of variations (COV) of 0.026 and 0.037 for the compression plus major axis bending and minor axis bending tests, respectively, representing both accurate and consistent predictions and confirming the validity of the FE models.

3.3 FE parametric studies

Based on the validated FE models, a series of parametric studies was carried out considering a wider range of specimen geometries. The parametric studies considered the two stainless steel grades employed in the experiments (304 and 2205), two loading arrangements (compression plus major and minor axis bending), three cross-section aspect ratios ($B\times H$ = 150×150, 150×250 and 150×300) and three cross-section classes (Class 1, 2 and 3 according to EN 1993-1-4 [24]). This has widened the cross-section slenderness range covered by the test specimens, where all the 304 specimens were Class 1 and all the 2205 specimens were Class 3. The lengths of the FE models were designed to give dimensionless slenderness values $\bar{\lambda} = \sqrt{Af_{0.2}/N_{cr}}$, where A

is the cross-sectional area and N_{cr} is the elastic buckling load, ranging from 0.5 to 2.0, in comparison with the more limited tested range, as given in Table 5, where $\bar{\lambda}_y$ and $\bar{\lambda}_z$ are the member slenderness values for major axis and minor axis buckling, respectively. For each of the above geometries, six load eccentricities e_0 were considered, giving a range of combinations of loading from pure bending ($\theta = 0^o$) to pure compression ($\theta = 90^o$), where θ is defined in Eq. (2). The input material parameters were defined based on the average tensile coupon test results from the experimental program. Initial geometric imperfections and residual stresses were also incorporated into the models. The geometric imperfections took the form of the first global eigenmode with an amplitude of $L_e/1000$, while the simplified distributions shown in Fig. 13 were employed to represent the residual stresses. In total, 1200 beam-column FE models were generated. The obtained FE results are used in conjunction with the experimental data to assess the existing design rules for stainless steel beam-columns with welded sections given in the European standard EN 1993-1-4 [24], the American Design Guide AISC DG 27 [26] and proposed in a recent study [17].

4. Assessment of current design guidance

In this section, the design methods for stainless steel beam-columns set out in the European standard EN 1993-1-4 [24] and American design guide AISC DG 27 [26], together with a recently proposed approach [17], are assessed against the obtained experimental and FE results. The assessment is presented on the basis of the ratio between the experimental (or numerical) failure load, N_u, and the corresponding resistance prediction from each design method, $N_{u,\text{pred}}$, as graphically illustrated in Fig. 17. A value of $N_u/N_{u,\text{pred}}$ greater than unity indicates a safe-sided prediction. It should be noted that $N_{u,\text{pred}}$ was obtained assuming proportional loading, following the same approach as in previous studies [17, 19]. The comparisons between the predictions from the different design methods for beam-column members with Class 1 and 2, and Class 3 cross-sections of the two different stainless steel grades are summarised in Table 6 for the loading case of compression plus major axis bending and Table 7 for compression plus minor axis bending, respectively. In the assessment, all calculations are based on the measured (or modelled) geometries and material properties, with all safety factors set to unity.

To describe the loading combination of axial load and bending moment, an angle parameter θ (Fig. 17) is adopted herein. The definition of θ is expressed in Eq. (2), where N_{Rd} is the axial compression resistance and M_{Rd} is the bending moment resistance, with $\theta = 0°$ corresponding to pure bending and $\theta = 90°$ corresponding to pure compression.

$$\theta = \tan^{-1}\left(\frac{N / N_{Rd}}{M / M_{Rd}}\right) \tag{2}$$

4.1 EN 1993-1-4

In the European design standard for stainless steel structures EN 1993-1-4 [24], beam-columns

should meet the requirements given by Eqs (3) and (4) for buckling about the major and minor axis, respectively.

$$\frac{N_{Ed}}{(N_{b,Rd})_{\min}} + k_y \left(\frac{M_{y,Ed} + N_{Ed} e_{Ny}}{\beta_{w,y} W_{pl,y} f_y / \gamma_{M1}} \right) \leq 1 \quad (3)$$

$$\frac{N_{Ed}}{(N_{b,Rd})_{\min}} + k_z \left(\frac{M_{z,Ed} + N_{Ed} e_{Nz}}{\beta_{w,z} W_{pl,z} f_y / \gamma_{M1}} \right) \leq 1 \quad (4)$$

In Eqs (3) and (4), the subscripts y and z denote buckling about the major and minor axis, respectively, N_{Ed} is the applied axial force, M_{Ed} is the applied end moment, e_N is the shift in neutral axis as a result of local buckling when the cross-section is subjected to uniform compression, with both $e_{N,y}$ and $e_{N,z}$ being equal to zero for the doubly symmetric I-sections studied herein, W_{pl} is the plastic modulus of the cross-section, $f_y = f_{0.2}$ is the 0.2% proof stress, γ_{M1} is the partial safety factor for member instability and is set to unity herein, β_W is the section modulus factor, which equals to 1.0 for Class 1 and 2 cross-sections and W_{el}/W_{pl} for Class 3 sections, and $(N_{b,Rd})_{min}$ relates to the lowest buckling resistances $N_{b,Rd}$ corresponding to a number of possible buckling modes. In this study, $(N_{b,Rd})_{min}$ in Eqs (3) and (4) corresponds to flexural buckling about the major and minor axis, respectively. It should be noted that for the members subjected to compression plus major axis bending, premature lateral-torsional buckling has been precluded in both the experiments (the end supports were pinned about the major axis but fixed about the minor axis) and the FE models (in addition to the end support condition as in the experiments, restraints against lateral displacement were provided at the mid-height cross-section of each model). The two k factors are the interaction factors defined as $k = 1.0 + 2(\bar{\lambda} - 0.5) N_{Ed}/N_{b,Rd}$ with the limitation of $1.2 \leq k \leq 1.2 + 2N_{Ed}/N_{b,Rd}$ for the two axes of buckling.

The test (or FE) to EC3 predicted failure load ratios $N_u/N_{u,EC3}$ are presented in Figs 18 and 19 for the beam-columns subjected to compression plus major axis bending and minor axis bending, respectively. Numerical comparisons, in terms of the mean values of the $N_u/N_{u,EC3}$ ratios and the coefficient of variation (COV), are also provided in Tables 6 and 7 for compression plus major and minor axis bending, respectively. For the two bending axes, the Eurocode predictions are shown to be generally safe-sided for both the 304 and 2205 stainless steel beam-columns. The duplex (2205) stainless steel beam-columns may be seen to exhibit somewhat better performance than the austenitic stainless steel members relative to the EC3 strength predictions. This is attributed primarily to the fact that the normalised residual stress amplitude is lower in the duplex stainless steel (2205) members ($0.6 f_{0.2}$) than in the austenitic stainless steel (304) members ($0.8 f_{0.2}$), resulting in higher normalised resistances, yet the same column buckling curve (with a plateau length $\bar{\lambda}_0 = 0.2$ and an imperfection factor $\alpha = 0.49$ and $\alpha = 0.76$ for major and minor axis buckling respectively) is employed for both grades. It may also be seen in Figs 18 and 19 that the capacity predictions for the members with Class 3 cross-sections are more conservative than those with Class 1 and Class 2 cross-sections for lower values of θ (i.e. as bending becomes more dominant). This can be explained by the different moment resistances assigned to the different section classes – the fully plastic moment M_{pl} for

Class 1 and Class 2 cross-sections and the first yield moment M_{el} for Class 3 cross-sections; this treatment neglects the fact that Class 3 cross-sections can reach higher moment capacities than M_{el}. In this regard, the findings in this study support the proposal of adopting a linear moment resistance transition from M_{pl} to M_{el} for Class 2 to Class 3 cross-sections in the next generation of Eurocode 3 [34].

4.2 AISC DG 27

In the recently published AISC design guide for stainless steel structures, AISC DG 27 [26], the design of stainless steel beam-columns refers to the corresponding provisions in the carbon steel standard AISC 360-10 [37], as expressed in Eqs (5) and (6).

$$\frac{P_r}{P_c}+\frac{8}{9}\left(\frac{M_{ry}}{M_{cy}}+\frac{M_{rz}}{M_{cz}}\right)\le 1 \qquad \text{for} \quad \frac{P_r}{P_c}\ge 0.2 \tag{5}$$

$$\frac{P_r}{2P_c}+\left(\frac{M_{ry}}{M_{cy}}+\frac{M_{rz}}{M_{cz}}\right)\le 1 \qquad \text{for} \quad \frac{P_r}{P_c}< 0.2 \tag{6}$$

where the subscripts y and z refer to the major and minor axis respectively, P_r is the design axial compression force, M_r is the design second-order bending moment, calculated as $P_r e_0/(1-P_r/P_e)$, where P_e is the Euler buckling load, P_c is the buckling resistance about the axis under consideration and M_c is the flexural resistance. It should be noted that P_c and M_c are dependent on the class of the cross-section, which can fall into three groups, namely the Compact (C), Non-compact (NC), and Slender (S) sections, according the local slenderness of the constituent plates [26, 35].

The test (or FE) to AISC predicted failure load ratios $N_u/N_{u,\mathrm{AISC}}$ are summarised in Tables 6 and 7, and graphically illustrated in Figs 20 and 21 for the cases of compression plus major axis bending and compression plus minor axis bending, respectively. In both loading cases, the AISC predictions show improved overall mean values of $N_u/N_{u,\mathrm{AISC}}$ compared to the Eurocode 3 predictions (as shown in Tables 6 and 7) , but are also rather scattered and with a number of results falling on the unsafe side (Figs 20 and 21). This can be attributed to 1) the adoption of a single buckling curve for instability about both the major and minor axes, and 2) the inaccuracy of the shape of the N-M interaction curves (Eqs (5) and (6)). Similar observations have also been made in a previous study [17].

4.3 Continuous Strength Method

The comparisons shown above and in numerous previous studies [17, 19-21, 27] have highlighted the need for improved design provisions for stainless steel beam-columns. Following the general format of the interaction curves employed in Eurocode 3, Greiner and Kettler [36] proposed new interaction factors for stainless steel beam-columns with Class 1 and 2 cross-sections, leading to more accurate resistance predictions. However, their proposals were based on the existing codified bending and column buckling resistance end points in the interaction curve, which are now known to be inaccurate. Addressing this shortcoming, in

recent design proposals for laser-welded stainless steel beam-columns [17], firstly, more accurate bending and column buckling resistance end points were defined and secondly, new interaction factors were derived. The bending moment end point utilises the Continuous Strength Method (CSM) [37], taking into account of the influence of strain hardening, while the column buckling end point employs suitable buckling curves, updated where necessary relative to the current EN 1993-1-4 provisions. The interaction factors were developed based on these revised end points.

The CSM interaction curves for stainless steel beam-columns under compression plus major and minor axis bending are expressed in Eqs (7) and (8) respectively.

$$\frac{N_{Ed}}{N_{b,y,Rd}} + k_{csm,y}\frac{M_{y,Ed}}{M_{csm,y,Rk}/\gamma_{M1}} \leq 1 \tag{7}$$

$$\frac{N_{Ed}}{N_{b,z,Rd}} + k_{csm,z}\frac{M_{z,Ed}}{M_{csm,z,Rk}/\gamma_{M1}} \leq 1 \tag{8}$$

where the subscripts y and z denote the major and minor axis respectively, $N_{b,\mathrm{Rd}}$ is column buckling resistance employing the bucking curve specified in EN 1993-1-4 [24] and verified in [38] (with $\bar{\lambda}_0 = 0.2$, $\alpha = 0.49$ for major axis buckling and $\alpha = 0.76$ for minor axis buckling), $M_{\mathrm{csm,Rk}}$ is the CSM bending moment resistance calculated from Eqs (9) and (10) for major and minor bending, respectively, with the definitions of E_{sh} and $\varepsilon_{csm}/\varepsilon_y$ detailed in [37], k_{csm} is the interaction factor devised on the basis of test and FE results in [17] following the approach used in [39, 40]. The derived interaction factors [17] are given by Eq. (11), where $\bar{\lambda}$ is the non-dimensional column slenderness and the parameters D_1, D_2 and D_3 are given in Table 8 for the different axes of bending. For the calculation of $k_{csm,\mathrm{y}}$, $\bar{\lambda} = \bar{\lambda}_y$ and $N_{b,\mathrm{Rd}} = N_{b,\mathrm{y,Rd}}$ while for the calculation of $k_{csm,\mathrm{z}}$, $\bar{\lambda} = \bar{\lambda}_z$ and $N_{b,\mathrm{Rd}} = N_{b,\mathrm{z,Rd}}$ in Eq. (11). It should be noted that the values in Table 8 were developed based on laser-welded stainless steel data [17], but are applied herein to conventionally welded sections; this is considered to be reasonable (and indeed is shown to be reasonable in the presented comparisons) since although the column buckling end point is different between laser-welded and conventionally welded sections, as accounted for in the selection of buckling curve, the general stability interaction response is expected to be similar.

$$M_{csm,y,Rk} = W_{pl,y} f_y \left[1 + \frac{E_{sh}}{E}\frac{W_{el,y}}{W_{pl,y}}\left(\frac{\varepsilon_{csm}}{\varepsilon_y} - 1\right) - \left(1 - \frac{W_{el,y}}{W_{pl,y}}\right)\Big/\left(\frac{\varepsilon_{csm}}{\varepsilon_y}\right)^2\right] \tag{9}$$

$$M_{csm,z,Rk} = W_{pl,z} f_y \left[1 + \frac{E_{sh}}{E}\frac{W_{el,z}}{W_{pl,z}}\left(\frac{\varepsilon_{csm}}{\varepsilon_y} - 1\right) - \left(1 - \frac{W_{el,z}}{W_{pl,z}}\right)\Big/\left(\frac{\varepsilon_{csm}}{\varepsilon_y}\right)^{1.2}\right] \tag{10}$$

$$k_{csm} = 1 + D_1\left(\bar{\lambda} - D_2\right)\frac{N_{Ed}}{N_{b,Rd}}, \text{ but } k_{csm} \leq 1 + D_1\left(D_3 - D_2\right)\frac{N_{Ed}}{N_{b,Rd}} \tag{11}$$

The CSM capacity predictions $N_{u,\mathrm{csm}}$ are compared with the test and FE results in Figs 22 and 23 for compression plus major and minor axis bending respectively, where the $N_u/N_{u,\mathrm{csm}}$ ratios

are plotted against θ. Mean values of $N_u/N_{u,\mathrm{csm}}$ and coefficients of variation are given in Table 6 for compression plus major axis bending and Table 7 for compression plus minor axis bending. From both the figures and the tables, the CSM may be seen to provide safe-sided capacity predictions that are substantially more accurate and less scattered than either of the existing codified methods.

To assess the suitability of the proposed CSM approach, reliability analyses in line with Annex D of EN 1990 [41] were carried out. The key parameters and results are summarised in Table 9, where b is the average of the ratios of the experimental (or FE) resistances to the theoretical (predicted) values, $k_{d,\mathrm{n}}$ is the design fractile factor for n data points of the dataset under consideration [41], V_δ is the coefficient of variation of the test and FE capacities relative to the resistance model, V_r is the combined coefficient of variation incorporating both model and basic variable (material and geometry) uncertainties and γ_{M1} is the required partial factor, which should be assessed against the EN 1993-1-4 [24] recommended value of 1.1. In the reliability analyses, the mean-to-nominal yield strength ratio (i.e. material over-strength factor) and the coefficients of variation of the yield strength $V_{\sigma 0.2}$ were taken as 1.3 and 0.06 for austenitic (304) stainless steel, and 1.1 and 0.03 for duplex (2205) stainless steel, respectively, as recommended by Afshan et al [42]. The coefficient of variation of the geometric properties V_g was taken as 0.05 [42].

It can be seen from Table 9 that the required values of γ_{M1} for the grade 304 stainless steel beam-columns under combined compression plus major axis bending and combined compression plus minor axis bending are 0.938 and 0.925, respectively, which are below the target value of 1.1. For the 2205 stainless steel beam-columns, higher γ_{M1} values of 0.990 for compression plus major axis bending and 0.991 for compression plus minor axis bending are indicated, which is attributed partly to the lower material over-strength factor (relative to the 304 stainless steel) for this material [42], but the required values remain below 1.1. It may therefore be concluded that the CSM based beam-column design approach may be applied in conjunction with γ_{M1} = 1.1. Similarly, the traditional EN 1993-1-4 end points may also conservatively (due to the lower end point in bending) be used with the proposed interaction factors.

5. Conclusions

A comprehensive experimental and numerical study into the response of welded I-section beam-columns made of grades 304 (EN 1.4301) and 2205 (EN 1.4462) stainless steel has been presented. The experimental program comprised tensile coupon tests, geometric imperfection measurements and beam-column tests. A total of twenty beam-columns, ten under combined compression plus major axis bending and ten under combined compression plus minor axis bending, were tested. Utilising the measured material and geometric properties of the test specimens, finite element (FE) models were developed firstly to replicate the experiments and secondly to perform parametric studies to generate results with a wider range of geometries. The obtained experimental and FE results were used in the assessment of current design provisions for stainless steel beam-columns, including EN 1993-1-4 [24], AISC DG 27 [26], and recent proposals set out in [17]. The EN 1993-1-4 resistance predictions were found to be

generally safe-sided but overly conservative and rather scattered. AISC DG 27 [26] provided improved accuracy in terms of the average capacity predictions, but with a large number of predictions falling on the unsafe side. The CSM [17], with improved end points and interaction factors provided the most accurate and least scattered resistance predictions, was shown to meet the reliability requirements set out in EN 1990 with γ_{M1} = 1.1 and is therefore recommended for inclusion in future revisions of Eurocode 3 and other international design codes.

Acknowledgement

This work was supported by the National Natural Science Foundation of China (Grant No. 51478019) and Beijing Excellent Talent Training Support (Grant No. 2017000026833ZK26).

References

[1] Gardner L, Bu Y, Francis P, Baddoo N R, Cashell K A, McCann F. Elevated temperature material properties of stainless steel reinforcing bar. Construction and Building Materials, 2016, 114:977-997.

[2] Afshan S, Rossi B, Gardner L. Strength enhancements in cold-formed structural sections - Part I: Material testing. Journal of Constructional Steel Research, 2013, 83:177 - 188.

[3] Rossi B, Afshan S, Gardner L. Strength enhancements in cold-formed structural sections - Part II: Predictive models. Journal of Constructional Steel Research 2013, 83: 189 - 196.

[4] Afshan S, Gardner L. Experimental study of cold-formed ferritic stainless steel hollow sections. Journal of Structural Engineering, ASCE, 2013, 139, 5:717 - 728.

[5] Arrayago I, Real E. Experimental Study on Ferritic stainless steel RHS and SHS cross-sectional resistance under combined loading. Structures, 2015, 4:69-79.

[6] Zhao O, Rossi B, Gardner L, Young B. Behaviour of structural stainless steel cross-sections under combined loading – Part I: Experimental study. Engineering Structures, 2015, 89:236-246.

[7] Zhao O, Rossi B, Gardner L, Young B. Behaviour of structural stainless steel cross-sections under combined loading – Part II: Numerical modelling and design approach. Engineering Structures, 2015, 89:247-259.

[8] Zhao O, Gardner L, Young B. Structural performance of stainless steel circular hollow sections under combined axial load and bending – Part 1: Experiments and numerical modelling. Thin-Walled Structures, 2015, 101:231–239.

[9] Zhao O, Gardner L, Young B. Structural performance of stainless steel circular hollow sections under combined axial load and bending – Part 2: Parametric studies and design. Thin-Walled Structures, 2015, 101:240–248.

[10] Zhao O, Rossi B, Gardner L, Young B. Experimental and numerical studies of ferritic stainless steel tubular cross sections under combined compression and bending. Journal of Structural Engineering, 2015, 142(2).

[11] Anbarasu M, Ashraf M. Behaviour and design of cold-formed lean duplex stainless steel lipped channel columns. Thin-Walled Structures, 2016, 104:106-115.

[12] Yang L, Zhao M H, Chan T M, Shang F, Xu D C. Flexural buckling of welded austenitic and duplex stainless steel I-section columns. Journal of Constructional Steel Research, 2016, 122:339-353.

[13] Yang L, Zhao M H, Xu D C, Shang F, Yuan H X, Wang Y Q, Zhang Y. Flexural buckling behavior of welded stainless steel box-section columns. Thin-Walled Structures, 2016, 104:185-197.
[14] Gardner L, Bu Y, Theofanous M. Laser-welded stainless steel I-sections: Residual stress measurements and column buckling tests. Engineering Structures, 2016, 127:536-548.
[15] Yuan H X, Wang Y Q, Gardner L, Shi Y J. Local–overall interactive buckling of welded stainless steel box section compression members. Engineering Structures, 2014, 67: 62-76.
[16] Zheng B F, Hua X, Shu G. Tests of cold-formed and welded stainless steel beam-columns. Journal of Constructional Steel Research, 2015, 111:1-10.
[17] Bu Y, Gardner, L. (in press) Experimental and numerical studies of laser-welded stainless steel I-section beam-columns. Engineering Structures.
[18] Burgan B A, Baddoo N R, Gilsenan K A. Structural design of stainless steel members comparison between Eurocode 3, Part1.4 and test results. Journal of Constructional Steel Research, 2000, 54:51-73.
[19] Zhao O, Gardner L, Young B. Buckling of ferritic stainless steel members under combined axial compression and bending. Journal of Constructional Steel Research, 2016, 117:35-48.
[20] Huang Y, Young B. Experimental investigation of cold-formed lean duplex stainless steel beam-columns. Thin-Walled Structures, 2014, 76(3):105-117.
[21] Lui W M, Ashraf M, Young B. Tests of cold-formed duplex stainless steel SHS beam–columns. Engineering Structures, 2014, 74:111-121.
[22] Anwar-Us-Saadat M, Ashraf M, Ahmed S. Behaviour and design of stainless steel slender cross-sections subjected to combined loading. Thin-Walled Structures, 2016, 104:225-237.
[23] Huang Y, Young B. Design of Cold-Formed Lean Duplex Stainless Steel Members in Combined Compression and Bending. Journal of Structural Engineering, 2014, 141(5).
[24] European Committee for Standardization. EN 1993-1-4. Eurocode 3: Design of steel structures- Part 1-4: General rules: Supplementary rules for stainless steels. London: BSI, 2006.
[25] American Society of Civil Engineers. SEI/ASCE 8-02: Specification for the Design of Cold-Formed Stainless Steel Structural Members. Virginia: ASCE, 2002.
[26] American Institute of Steel Construction (AISC). AISC Design Guide 27: Structural Stainless Steel. Chicago, Illinois, USA, 2013.
[27] Zhao O, Gardner L, Young B. Behaviour and design of stainless steel SHS and RHS beam-columns. Thin-Walled Structures, 2016, 106:330-345.
[28] GB/T 222-2006. Permissible tolerances for chemical composition of steel products. 2006. (in Chinese)
[29] GB/T 20878-2007. Stainless and heat-resisting steels-Designation and chemical composition. 2007. (in Chinese)
[30] European Committee for Standardization, EN ISO 6892-1-2009: Metallic Materials Tensile Testing — Part 1: Method of Test at Ambient Temperature, BSI, Brussels, 2009.
[31] Wang J, Gardner L. Flexural buckling of hot-finished high strength steel square and rectangular hollow section columns. Journal of Structural Engineering, ASCE, 2017, 143, 6: 04017028.
[32] ABAQUS. Standard user's manual volume I–III and ABAQUS CAE manual. Version 6.14,

Hibbitt and Karlsson and Sorensen Inc. 2014.
[33] Yuan H X, Wang Y Q, Shi Y J, Gardner L. Residual stress distributions in welded stainless steel sections. Thin-Walled Structures, 2014, 79:38-51.
[34] Taras A, Unterweger H. New developments for the cross-section and stability design of steel members on the basis of EN 1993-1-1. Bauingenieur, 89:405-415.
[35] ANSI/AISC 360-10. Specification for structural steel buildings, Chicago, 2010.
[36] Greiner R, Kettler M. Interaction of bending and axial compression of stainless steel members. Journal of Constructional Steel Research, 2008, 64:1217-1224.
[37] Afshan S, Gardner L. The continuous strength method for structural stainless steel design. Thin-Walled Structures, 2013, 68:42-49.
[38] Bu Y, Gardner L. Finite element modelling and design of welded stainless steel I-section columns. Journal of Constructional Steel Research, 2019, 152:57-67.
[39] Greiner R, Lindner J. Interaction formulae for members subjected to bending and axial compression in EUROCODE 3 – the Method 2 approach. Journal of Constructional Steel Research, 2006, 62(8):757-70.
[40] Boissonnade N, Greiner R, Jaspart J P, Lindner J. Rules for Member Stability in EN 1993-1-1: Background documentation and design guidelines. ECCS European Convention for Constructional Steelwork, 2006.
[41] European Committee for Standardization. EN 1990: 2002+A1:2005. Basis of structural design, BSI, Brussels, 2005.
[42] Afshan S, Francis P, Baddoo N, Gardner L. Reliability analysis of structural stainless steel design provisions. Journal of Constructional Steel Research, 2015, 114:293-304.

Figures

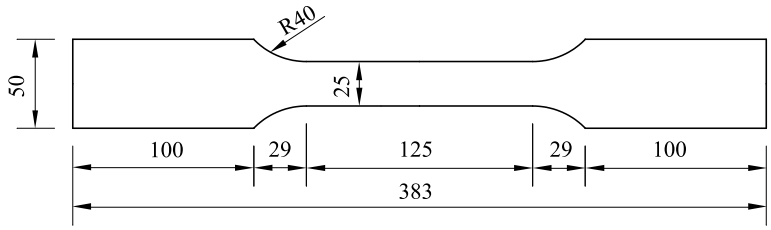

Fig. 1 Dimensions of tensile coupons (in mm)

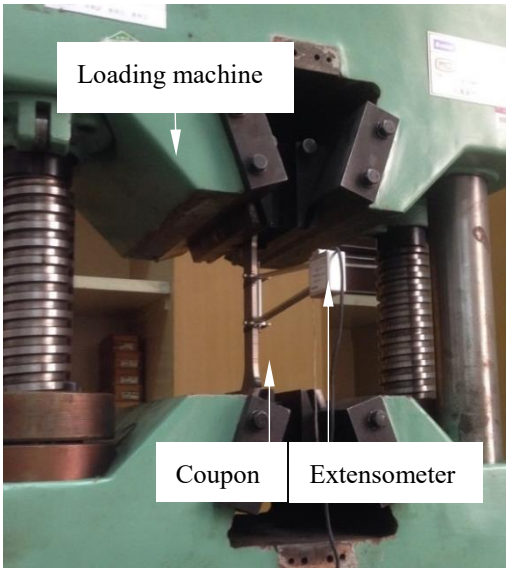

Fig. 2 Tensile coupon test set-up

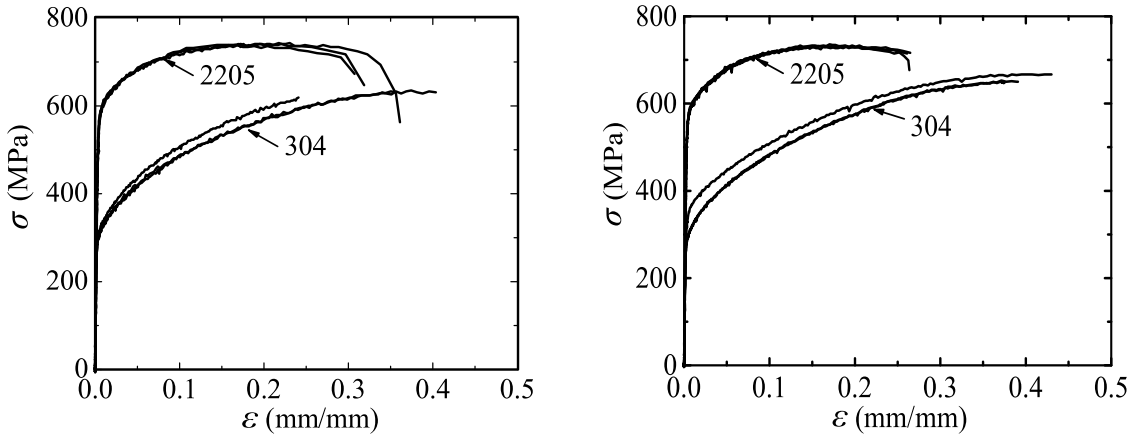

(a) 6 mm (b) 10 mm

Fig. 3 Measured stress-strain curves of (a) 6 mm and (b) 10 mm thick stainless steel material.

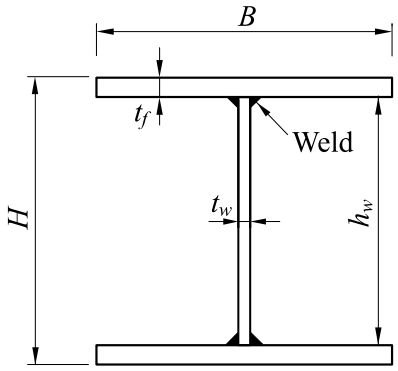

Fig. 4 Notations for cross-sectional dimensions

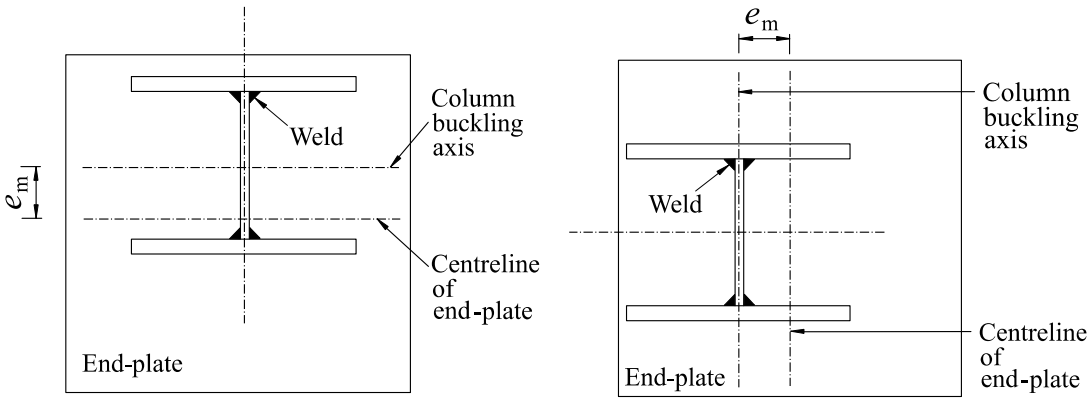

(a) Buckling about major axis (b) Buckling about minor axis

Fig. 5 Relative position of specimens on end-plates

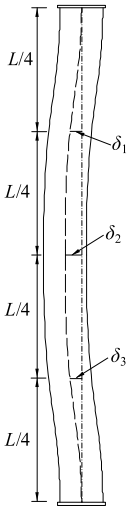

Fig. 6 Initial geometric imperfection profile

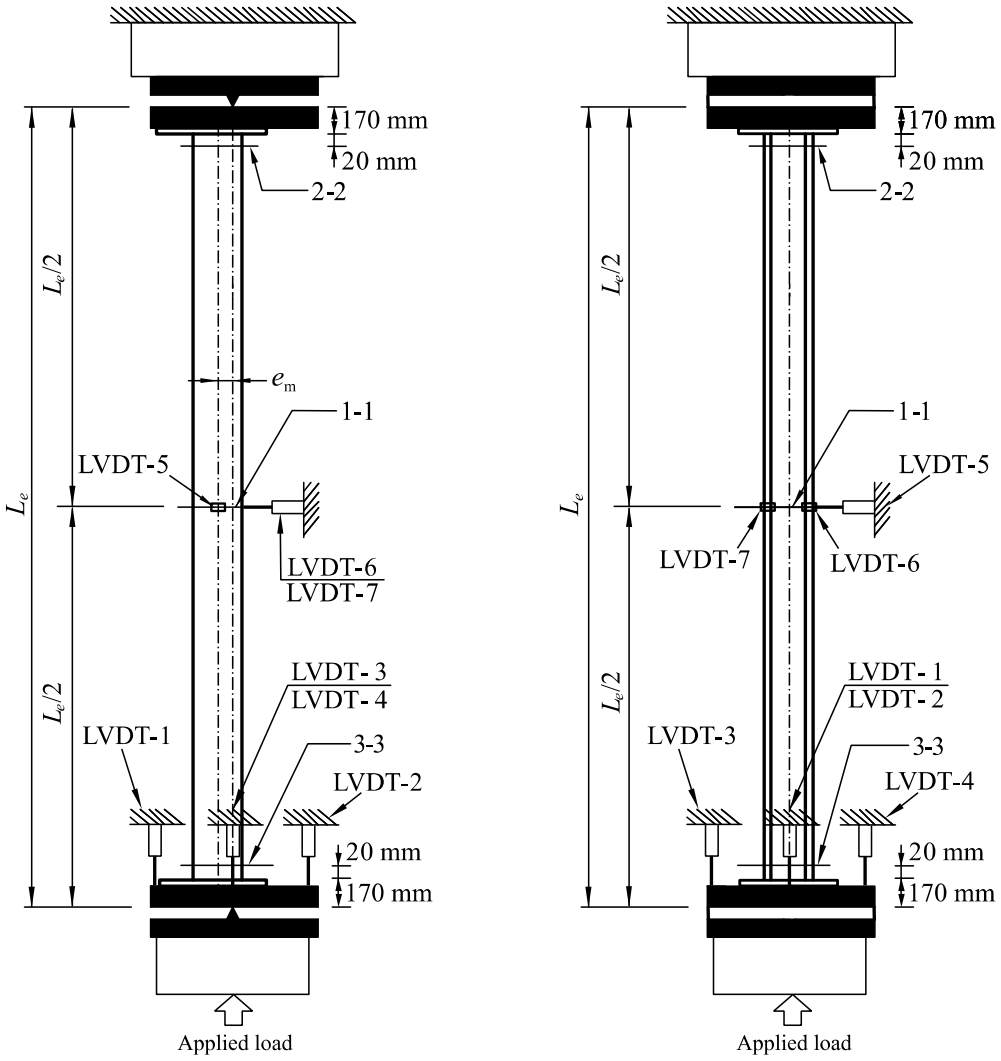

(a) Front view (b) Side view

Fig. 7 Test set-up

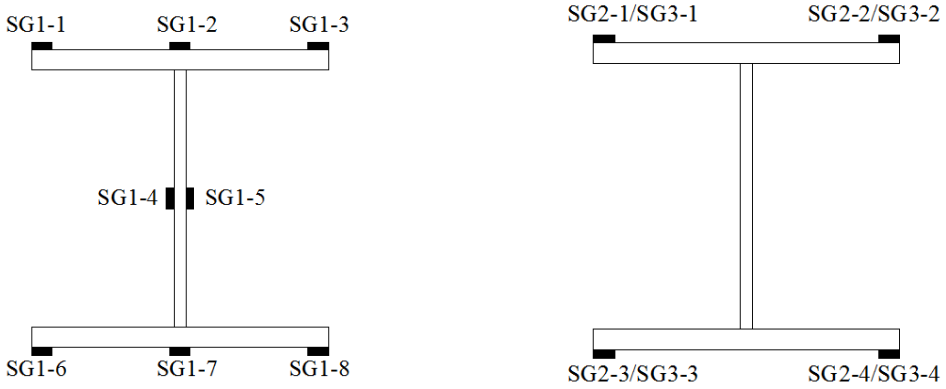

(a) Mid-height (section 1-1 in Fig. 7) (b) Column end (sections 2-2 and 3-3 in Fig. 7)

Fig. 8 Positions of strain gauges on specimen cross-sections

(a) I 304-2500 specimen failing about the major axis

(b) H 304-2500 specimen failing about the minor axis

Fig. 9 Typical failure modes of beam-column test specimens

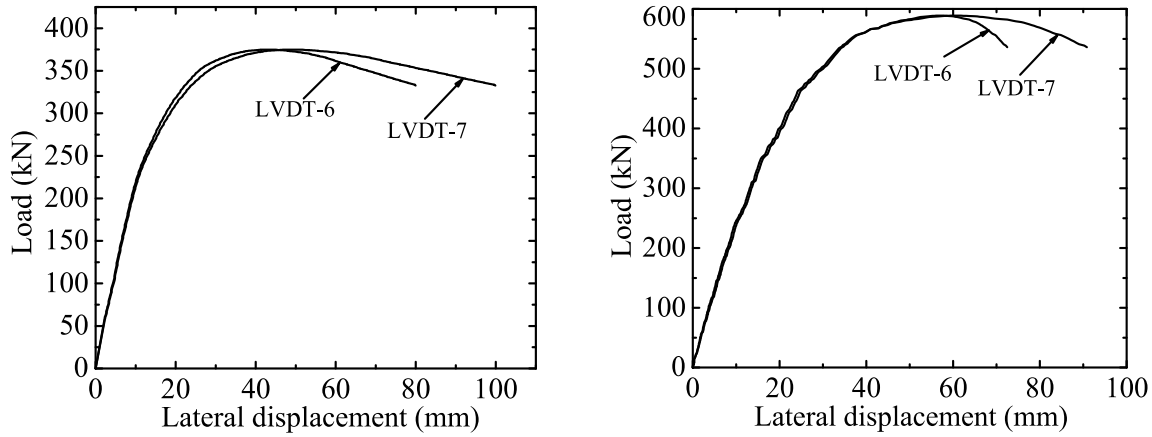

(a) I 304-3000-1 specimen (b) I 2205-3000-1 specimen

Fig. 10 Comparison of LVDT-6 and LVDT-7 readings in specimens bent about the major axis

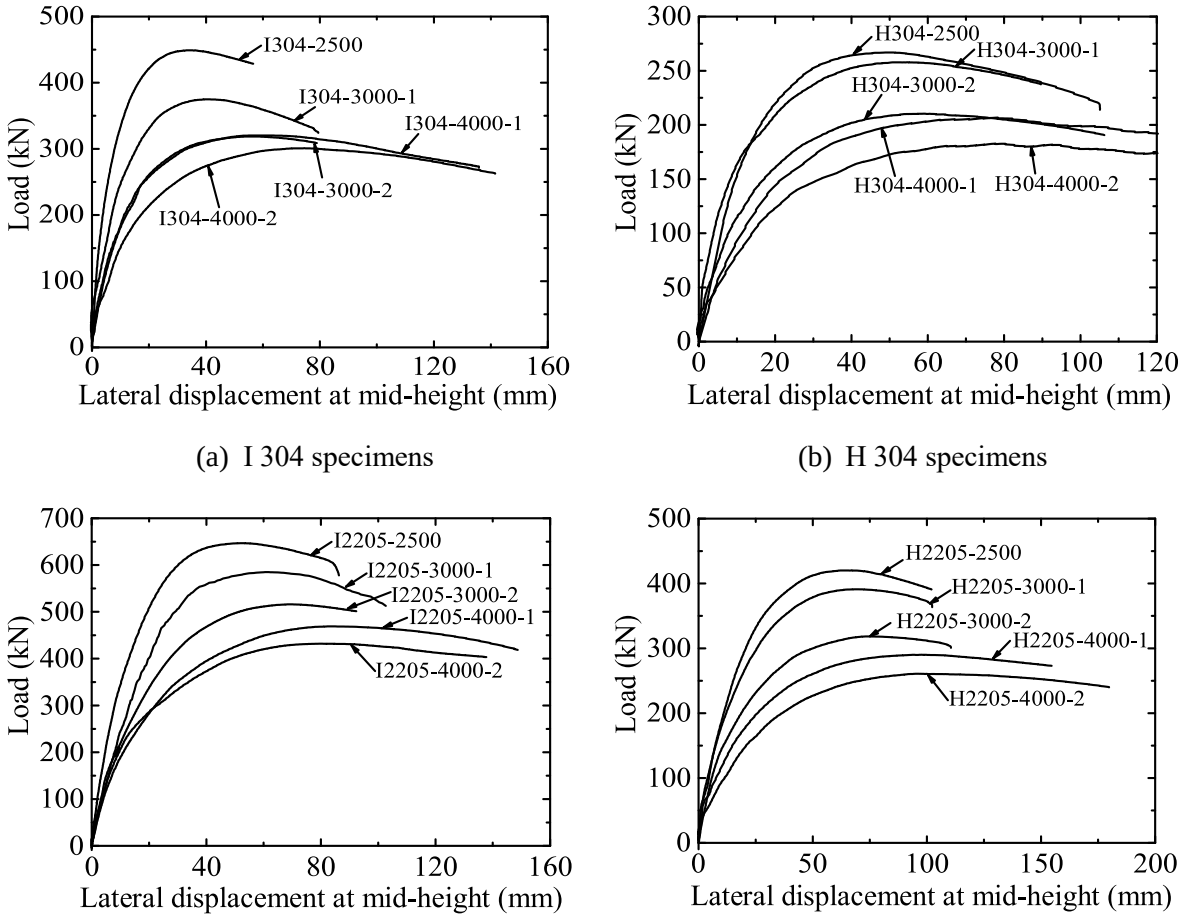

(a) I 304 specimens (b) H 304 specimens

(c) I 2205 specimens (d) H 2205 specimens

Fig. 11 Load versus lateral displacement at mid-height of the tested beam-columns

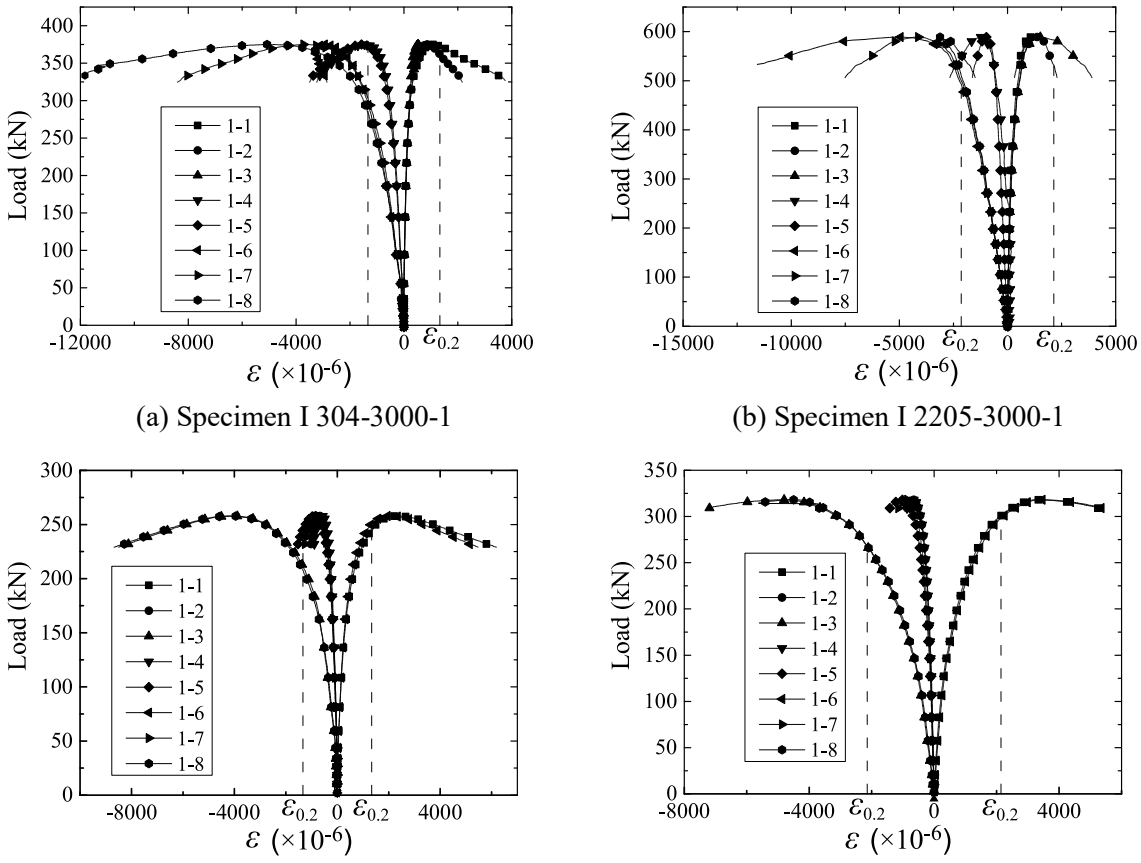

(a) Specimen I 304-3000-1

(b) Specimen I 2205-3000-1

(c) Specimen H 304-3000-1

(d) Specimen H 2205-3000-2

Fig. 12 Load versus strain at the mid-height cross-section of sample beam-column test specimens

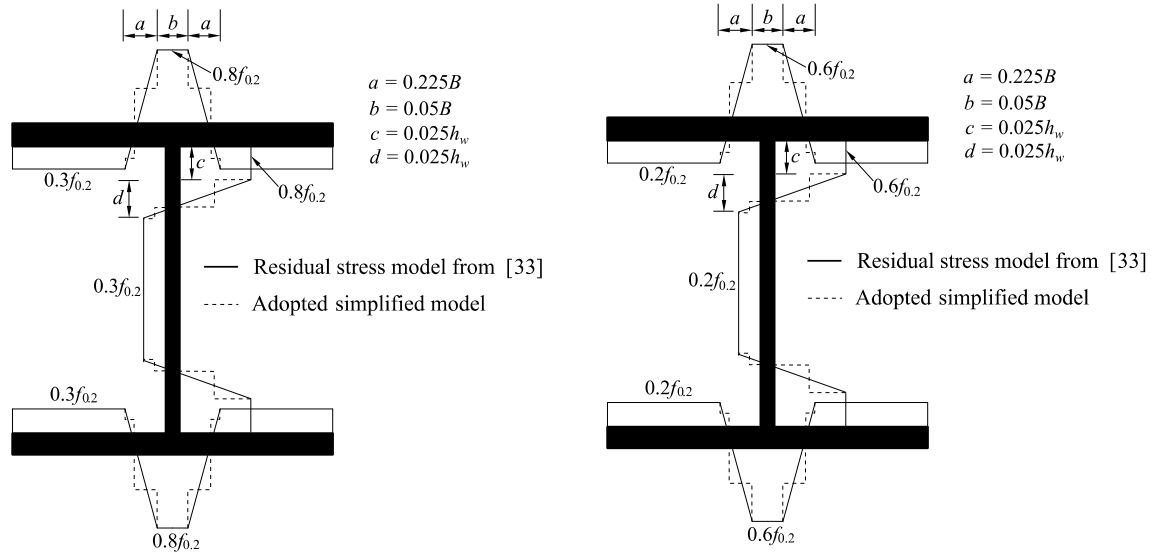

(a) Austenitic stainless steel (Grade 304)

(b) Duplex stainless steel (Grade 2205)

Fig. 13 Residual stress models adopted in numerical simulations

(a) Specimen I 304-3000-1 (b) Specimen H 304-3000-1

Fig. 14 Comparison between typical failure modes obtained from FE models and tests

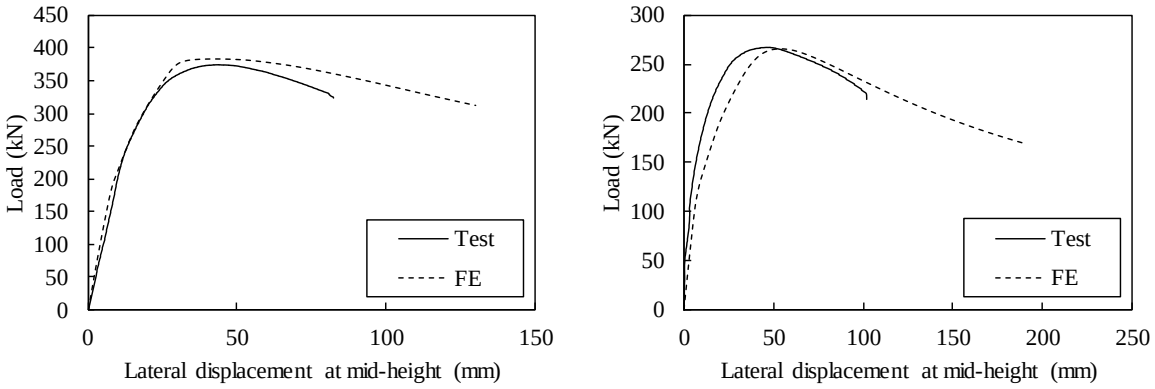

(a) Specimen I 304-3000-1 (b) Specimen H 304-2500

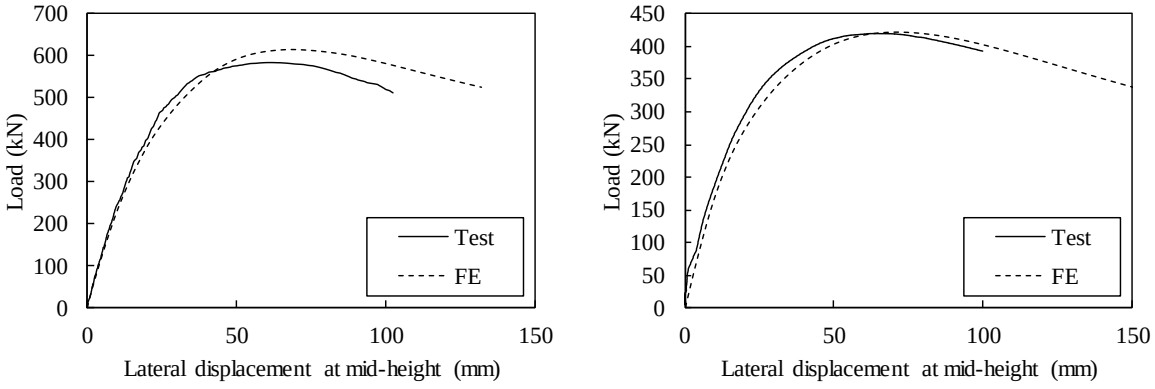

(c) Specimen I 2205-3000-1 (d) Specimen H 2205-2500

Fig. 15 Comparison of FE and test load versus mid-height lateral displacement curves

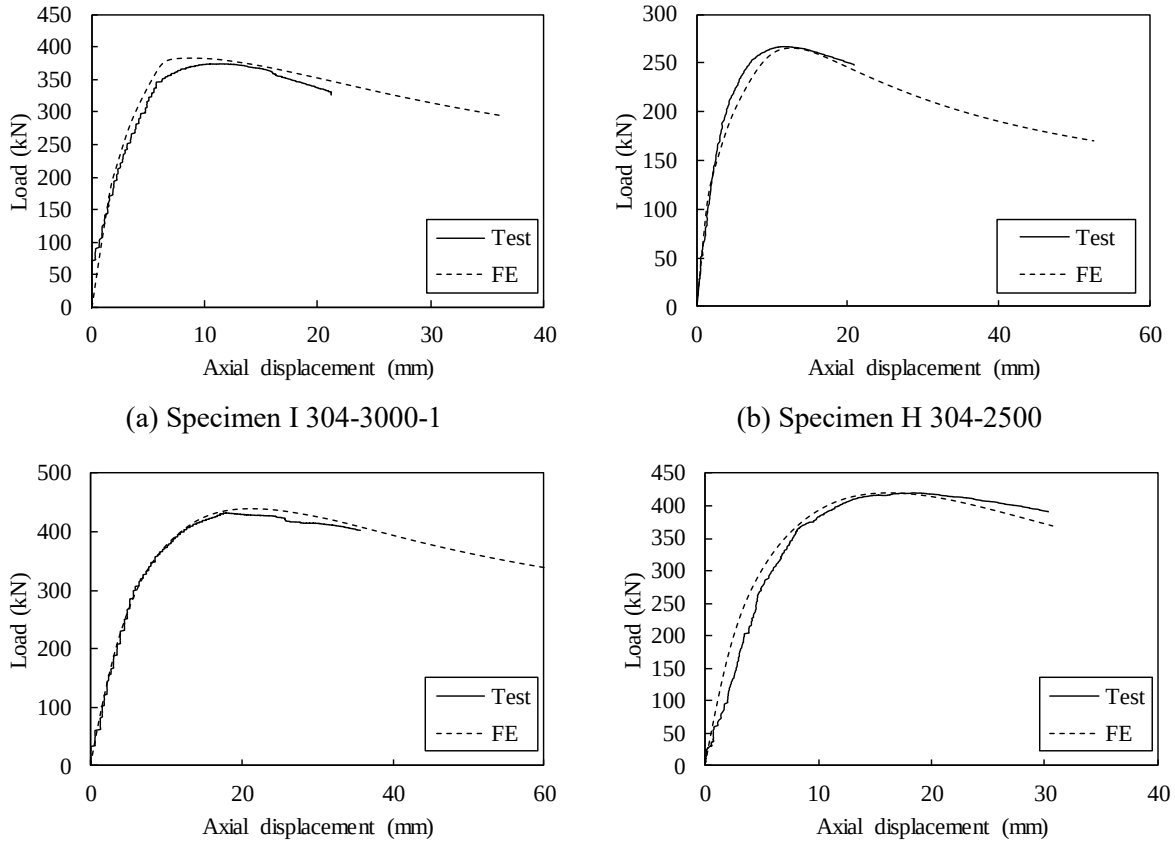

Fig. 16 Comparison of FE and test load versus axial displacement curves

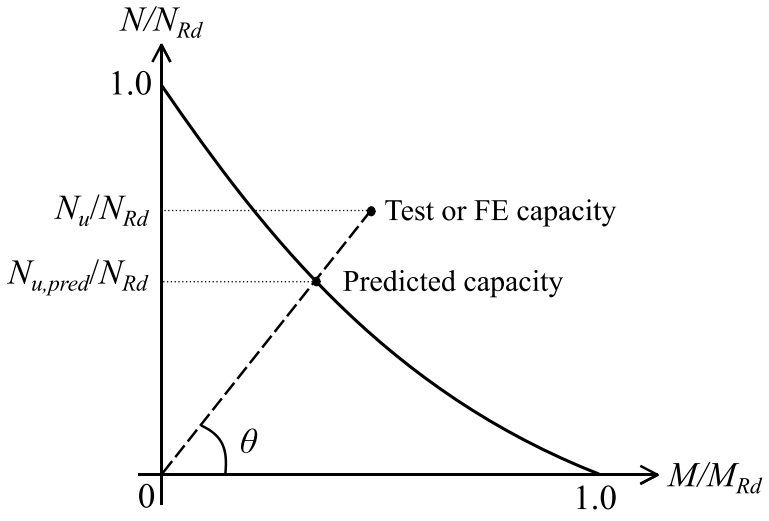

Fig. 17 Definition of θ on axial load-moment interaction curve

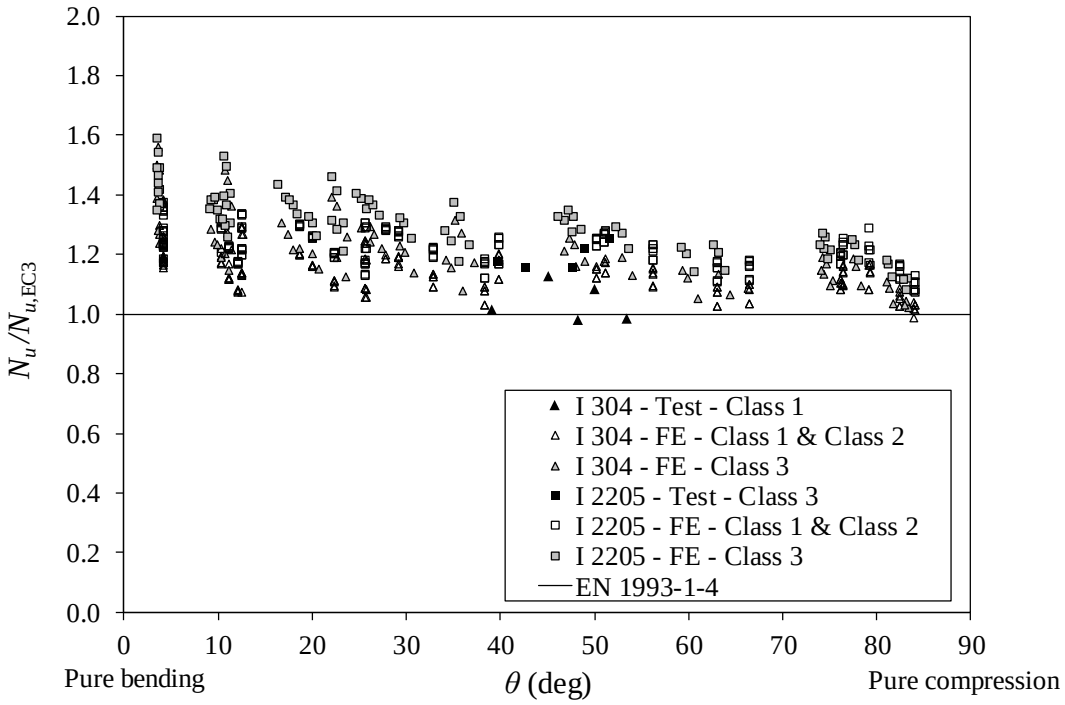

Fig. 18 Comparisons of EN 1993-1-4 capacity predictions with test and FE results for beam-columns under combined compression and major axis bending

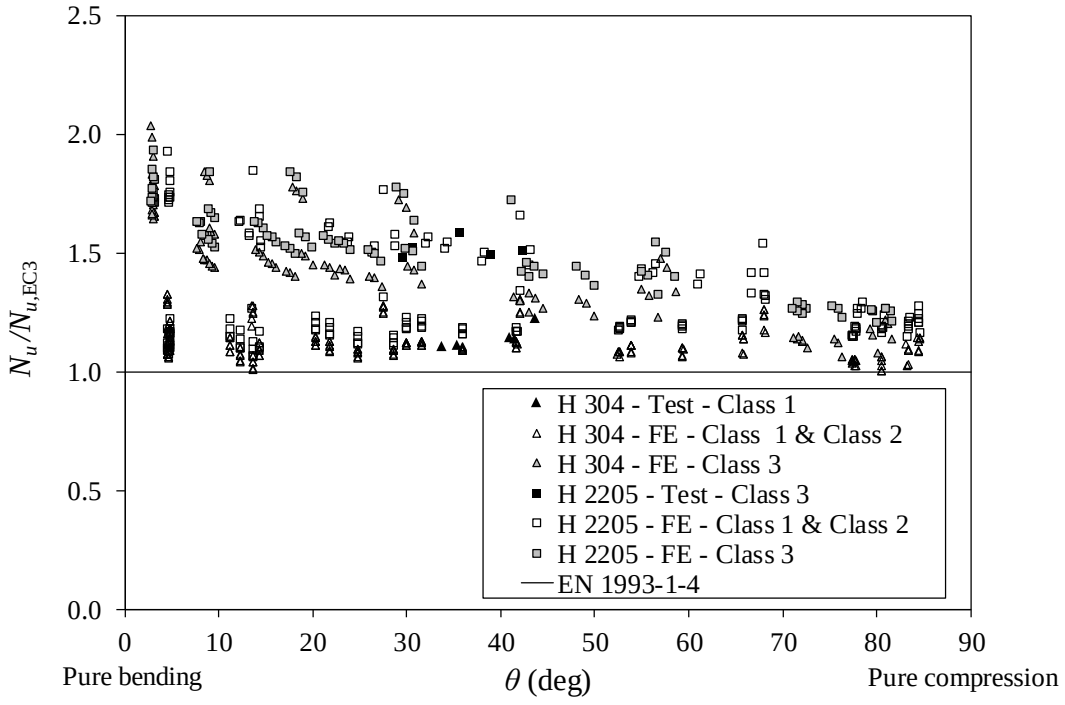

Fig. 19 Comparisons of EN 1993-1-4 capacity predictions with test and FE results for beam-columns under combined compression and minor axis bending

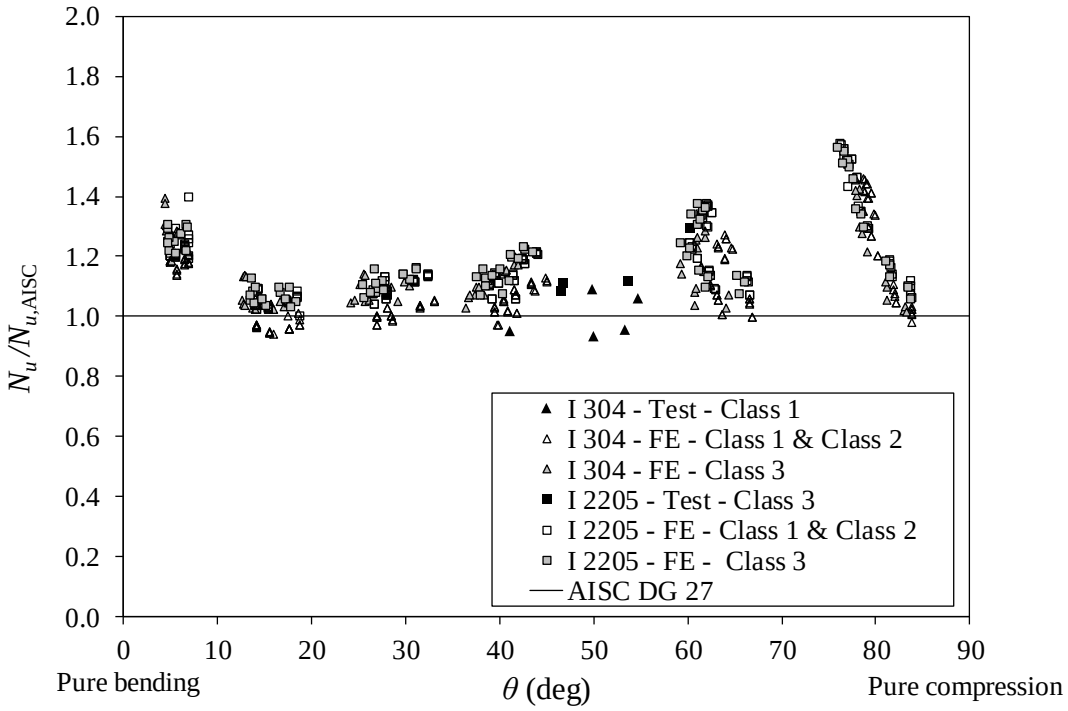

Fig. 20 Comparisons of AISC capacity predictions with test and FE results for beam-columns under combined compression and major axis bending

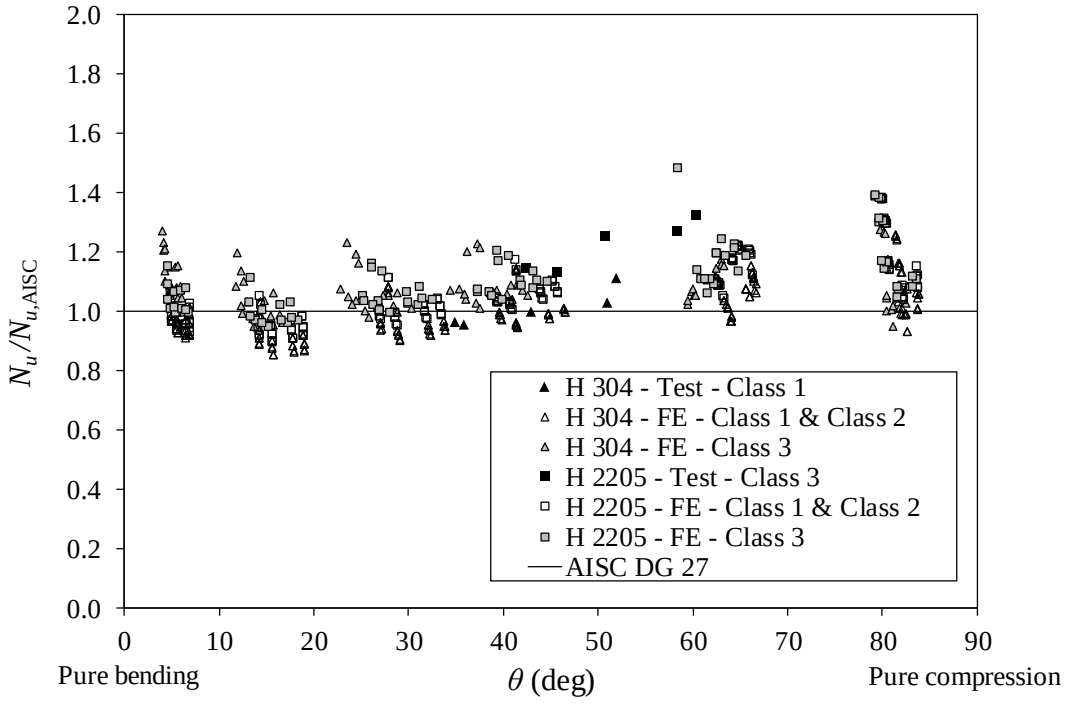

Fig. 21 Comparisons of AISC capacity predictions with test and FE results for beam-columns under combined compression and minor axis bending

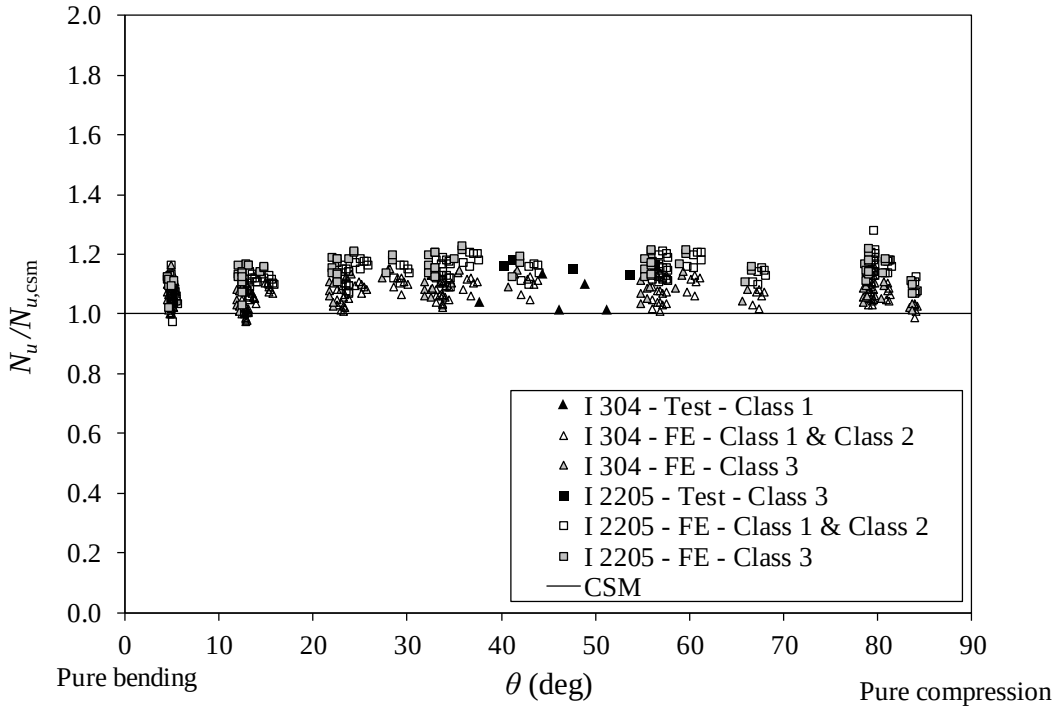

Fig. 22 Comparisons of CSM capacity predictions with test and FE results for beam-columns under combined compression and major axis bending

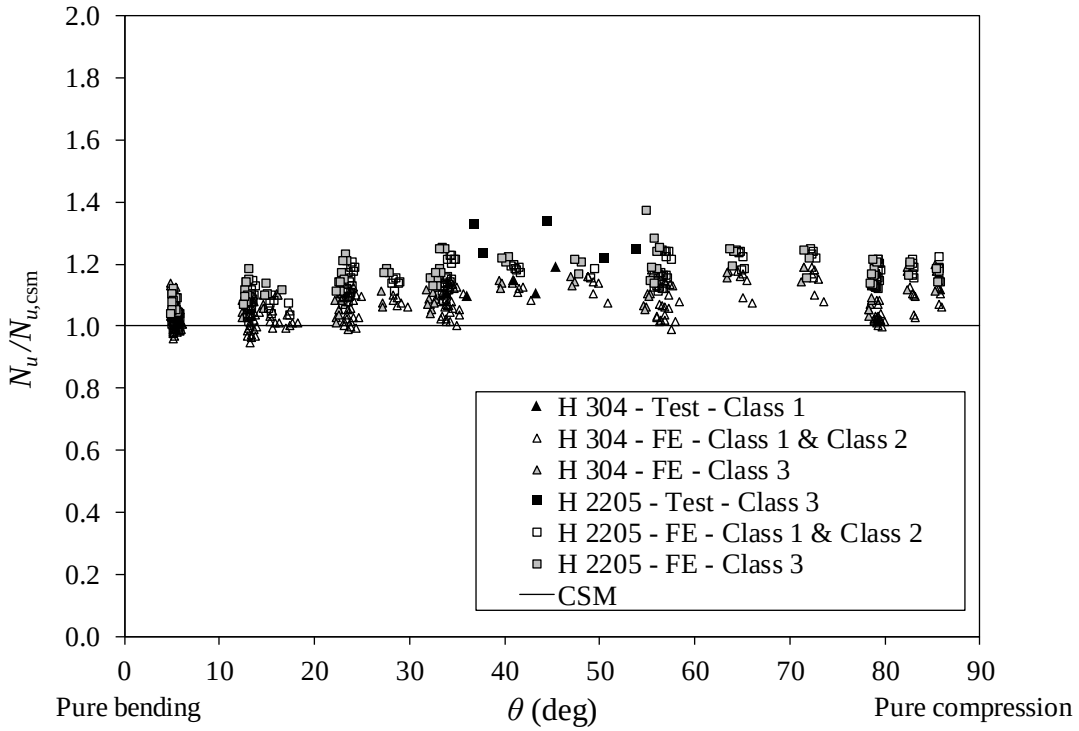

Fig. 23 Comparisons of CSM capacity predictions with test and FE results for beam-columns under combined compression and minor axis bending

Tables

Table 1 Chemical composition from mill certificate

Grade	Nominal thickness	Cr (%)	Mn (%)	Ni (%)	P (%)	Si (%)	C (‰)	S (‰)	Mo (%)	N (%)
Grade 304	6 mm	18.50	1.04	8.35	0.033	0.52	0.40	0.03	-	-
(EN 1.4301)	10 mm	18.38	0.98	8.24	0.026	0.48	0.48	0.03	-	-
Grade 2205	6 mm	22.93	1.18	5.64	0.022	0.56	0.26	<0.01	3.22	0.17
(EN 1.4462)	10 mm	22.88	0.99	5.70	0.022	0.51	0.22	<0.01	3.24	0.17

Table 2 Average measured tensile material properties

Grade	t (mm)	E (MPa)	$f_{0.2}$ (MPa)	f_u (MPa)	ε_u (%)	ε_f (%)	n
Grade 304	5.85	200000	298.2	630.7	30.0	57.0	6.1
(EN 1.4301)	10.02	195300	300.0	656.0	38.0	56.7	6.6
Grade 2205	5.87	205000	568.0	740.9	20.0	36.4	6.9
(EN 1.4462)	9.91	200300	566.7	733.0	16.0	36.6	7.8

Table 3 Measurements of specimen geometries

Specimen	Bending axis	e_m (mm)	H (mm)	B (mm)	t_f (mm)	t_w (mm)	L (mm)	L_e (mm)
I 304-2500	Major	40.7	119.5	149.7	10.02	5.85	2496	2836
I 304-3000-1	Major	50.3	120.1	150.0	10.02	5.85	2996	3336
I 304-3000-2	Major	70.7	117.3	149.6	10.02	5.85	2999	3339
I 304-4000-1	Major	50.1	118.5	149.8	10.02	5.85	4016	4356
I 304-4000-2	Major	61.1	117.3	149.8	10.02	5.85	4015	4355
I 2205-2500	Major	57.9	119.3	149.6	9.91	5.87	2498	2838
I 2205-3000-1	Major	50.9	120.0	150.0	9.91	5.87	2998	3338
I 2205-3000-2	Major	70.1	118.4	149.3	9.91	5.87	2998	3338
I 2205-4000-1	Major	50.2	118.3	149.9	9.91	5.87	3996	4336
I 2205-4000-2	Major	56.5	118.3	149.7	9.91	5.87	3997	4337
H 304-2500	Minor	57.2	138.6	149.6	10.02	5.85	2497	2837
H 304-3000-1	Minor	48.8	138.3	149.7	10.02	5.85	2995	3335
H 304-3000-2	Minor	70.3	138.8	149.6	10.02	5.85	2996	3336
H 304-4000-1	Minor	50.2	138.6	150.0	10.02	5.85	3996	4336
H 304-4000-2	Minor	56.8	139.9	149.8	10.02	5.85	3995	4335
H 2205-2500	Minor	56.0	138.0	149.5	9.91	5.87	2501	2841
H 2205-3000-1	Minor	49.7	139.0	149.5	9.91	5.87	2997	3337
H 2205-3000-2	Minor	70.4	138.2	149.6	9.91	5.87	2996	3336
H 2205-4000-1	Minor	48.8	139.7	149.8	9.91	5.87	3997	4337
H 2205-4000-2	Minor	60.8	136.7	149.8	9.91	5.87	3999	4339

Table 4 Measured initial geometric imperfections (in mm)

Specimen	δ_1	δ_2	δ_3	δ_0
I 304-2500	-0.109	5.048	0.439	5.048
I 304-3000-1	5.470	2.590	1.580	5.470
I 304-3000-2	-1.729	-0.153	-0.306	1.729
I 304-4000-1	-4.175	-0.200	1.055	4.175
I 304-4000-2	-2.849	-1.868	0.354	2.849
I 2205-2500	3.734	2.553	0.916	3.734
I 2205-3000-1	2.105	0.465	1.220	2.105
I 2205-3000-2	-2.544	-1.333	-1.321	2.544
I 2205-4000-1	2.781	0.358	2.494	2.781
I 2205-4000-2	-0.063	-0.555	-0.808	0.808
H 304-2500	-0.833	-1.405	0.642	1.405
H 304-3000-1	-0.846	1.718	2.001	2.001
H 304-3000-2	1.837	1.845	2.422	2.422
H 304-4000-1	24.953	13.870	10.158	24.953
H 304-4000-2	0.203	-1.680	-1.598	1.680
H 2205-2500	-0.015	-0.830	-0.575	0.830
H 2205-3000-1	-0.811	-0.368	-0.074	0.811
H 2205-3000-2	-0.560	-5.690	-6.870	6.870
H 2205-4000-1	0.614	2.427	0.181	2.427
H 2205-4000-2	1.191	0.263	-1.256	1.256

Table 5 Summary of beam-column test and FE results

Specimen	e_0 (mm)	$\bar{\lambda}_y$ or $\bar{\lambda}_z$*	$N_{u,\text{exp}}$ (kN)	$N_{u,\text{FE}}$ (kN)	$N_{u,\text{FE}}/N_{u,\text{exp}}$
I 304-2500	41.1	0.69	454.0	458.0	1.009
I 304-3000-1	52.1	0.80	376.4	382.7	1.017
I 304-3000-2	74.5	0.82	321.1	315.6	0.983
I 304-4000-1	52.5	1.06	324.7	313.3	0.965
I 304-4000-2	60.3	1.07	306.3	291.5	0.952
I 2205-2500	60.2	0.95	649.5	654.5	1.008
I 2205-3000-1	52.8	1.11	597.8	616.0	1.031
I 2205-3000-2	72.2	1.12	516.6	529.7	1.025
I 2205-4000-1	51.4	1.46	472.4	468.9	0.993
I 2205-4000-2	61.7	1.46	439.2	440.2	1.002
				Mean	0.998
				COV	0.026
H 304-2500	61.4	0.91	269.4	265.1	0.984
H 304-3000-1	52.3	1.07	262.0	249.2	0.951
H 304-3000-2	71.4	1.07	217.7	214.8	0.987
H 304-4000-1	54.8	1.38	210.3	187.9	0.893
H 304-4000-2	59.9	1.39	188.2	181.0	0.962
H 2205-2500	60.2	1.25	428.1	417.7	0.976
H 2205-3000-1	53.7	1.47	398.6	375.7	0.943
H 2205-3000-2	72.1	1.47	324.7	332.8	1.025
H 2205-4000-1	53.2	1.91	291.5	284.7	0.977
H 2205-4000-2	61.7	1.90	269.4	270.4	1.004
				Mean	0.970
				COV	0.037

* $\bar{\lambda}_y$ is the dimensionless slenderness for specimens buckling about the major axis (I specimens) and $\bar{\lambda}_z$ is the dimensionless slenderness for specimens buckling about the minor axis (H specimens)

Table 6 Comparison of test and FE results with predicted strengths for beam-columns under compression plus major axis bending

		$N_u/N_{u,\text{EC3}}$		$N_u/N_{u,\text{AISC}}$		$N_u/N_{u,\text{csm}}$	
Grade	Section class	Mean	COV	Mean	COV	Mean	COV
I 304	Class 1 and 2	1.141	0.069	1.103	0.115	1.063	0.037
	Class 3	1.220	0.096	1.159	0.107	1.092	0.037
I 2205	Class 1 and 2	1.224	0.051	1.184	0.111	1.127	0.044
	Class 3	1.307	0.080	1.192	0.106	1.153	0.035
Overall		1.211	0.085	1.155	0.115	1.106	0.050

Table 7 Comparison of test and FE results with predicted strengths for beam-columns under compression plus minor axis bending

		$N_u/N_{u,\mathrm{EC3}}$		$N_u/N_{u,\mathrm{AISC}}$		$N_u/N_{u,\mathrm{csm}}$	
Grade	Section class	Mean	COV	Mean	COV	Mean	COV
H 304	Class 1 and 2	1.125	0.066	1.003	0.087	1.055	0.053
	Class 3	1.467	0.149	1.094	0.079	1.108	0.058
H 2205	Class 1 and 2	1.298	0.156	1.064	0.107	1.129	0.060
	Class 3	1.538	0.114	1.108	0.098	1.167	0.056
Overall		1.307	0.177	1.054	0.101	1.104	0.067

Table 8 Interaction curve coefficients used in the CSM design approach [17]

Loading cases	D_1	D_2	D_3
Compression plus major axis bending	2.50	0.35	1.00
Compression plus minor axis bending	2.80	0.50	1.20

Table 9 Summary of reliability analysis results for the CSM design approach.

Loading cases	Grade	n	b	$k_{d,\mathrm{n}}$	V_δ	γ_{M1}
Compression plus major axis bending	304	238	1.076	3.132	0.040	0.939
	2205	266	1.149	3.127	0.043	0.990
Compression plus minor axis bending	304	275	1.117	3.126	0.054	0.925
	2205	251	1.195	3.129	0.061	0.991